Supplemental Figures

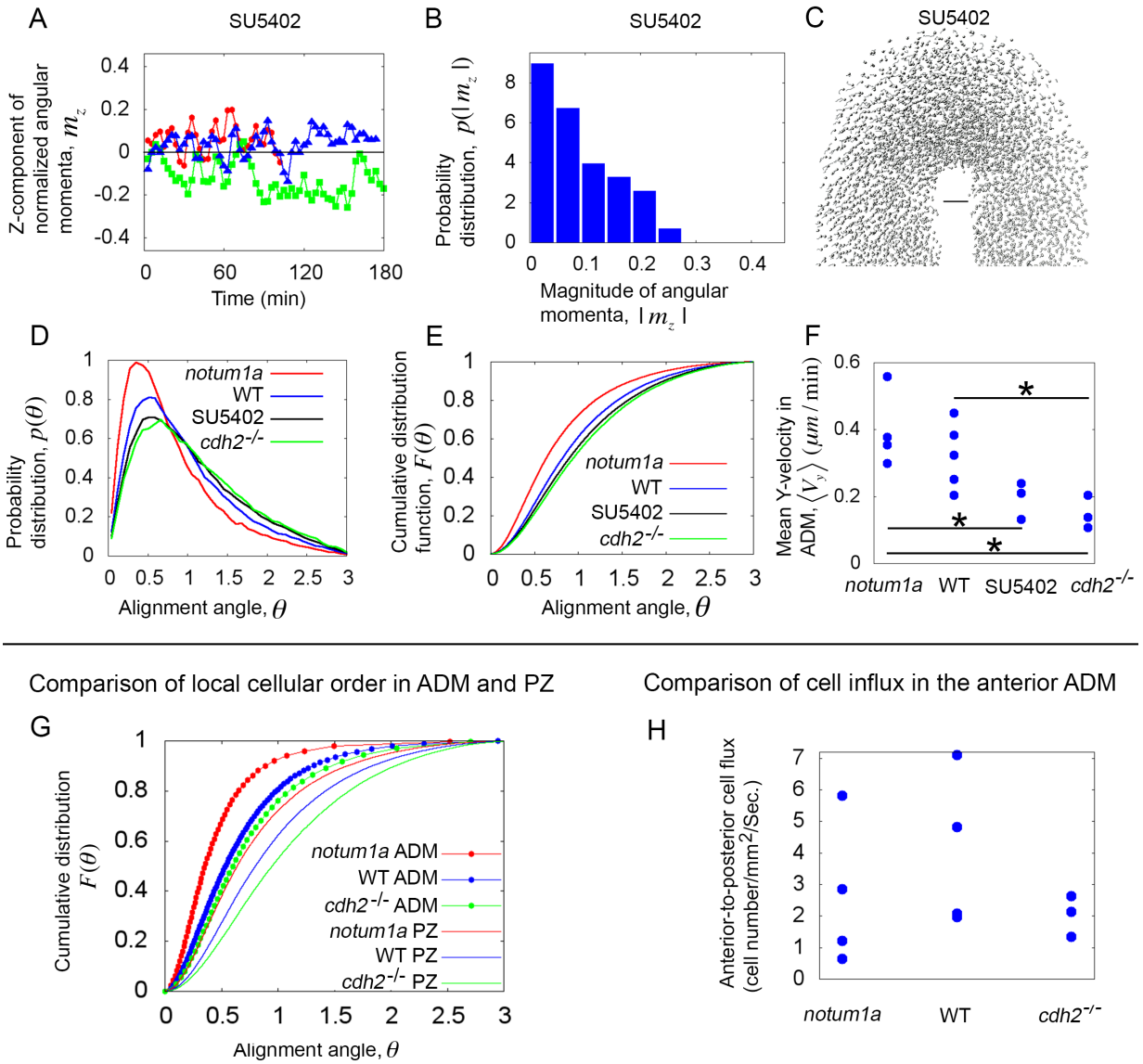

Figure S1. Supplemental analysis of in vivo cell motion; related to Figure 3. (A-C) Analysis of embryos treated with the Fgfr inhibitor SU5402. **(A)** The Z-component of the angular momentum inside the PZ versus time. **(B)** The probability distribution of the angular momentum. **(C)** Experimental image of cell motion with nuclear trails drawn from last few timepoints. Scale bar: 30 microns. **(D)** Probability distribution functions of the alignment angles of the PZ cells. **(E)** Cumulative distribution functions (CDF) of the alignment angles of the PZ cells, showing distinct states of cellular order for different phenotypes. **(F)** Average of net anterior-to-posterior velocity components per cell inside the ADM for different phenotypes. The p-values are calculated using a two-sample T-test with unequal variance, and "*" denotes p<0.05. **(G)** Comparison of CDFs of alignment angles inside the ADM and PZ illustrates the difference in order of the epithelium (ADM) and mesenchyme (PZ). (H) Anterior-to-posterior cell flux through a transverse section of the ADM, measured at 50 microns from the anterior end of the ADM. There is no significant difference in the fluxes among different phenotypes.

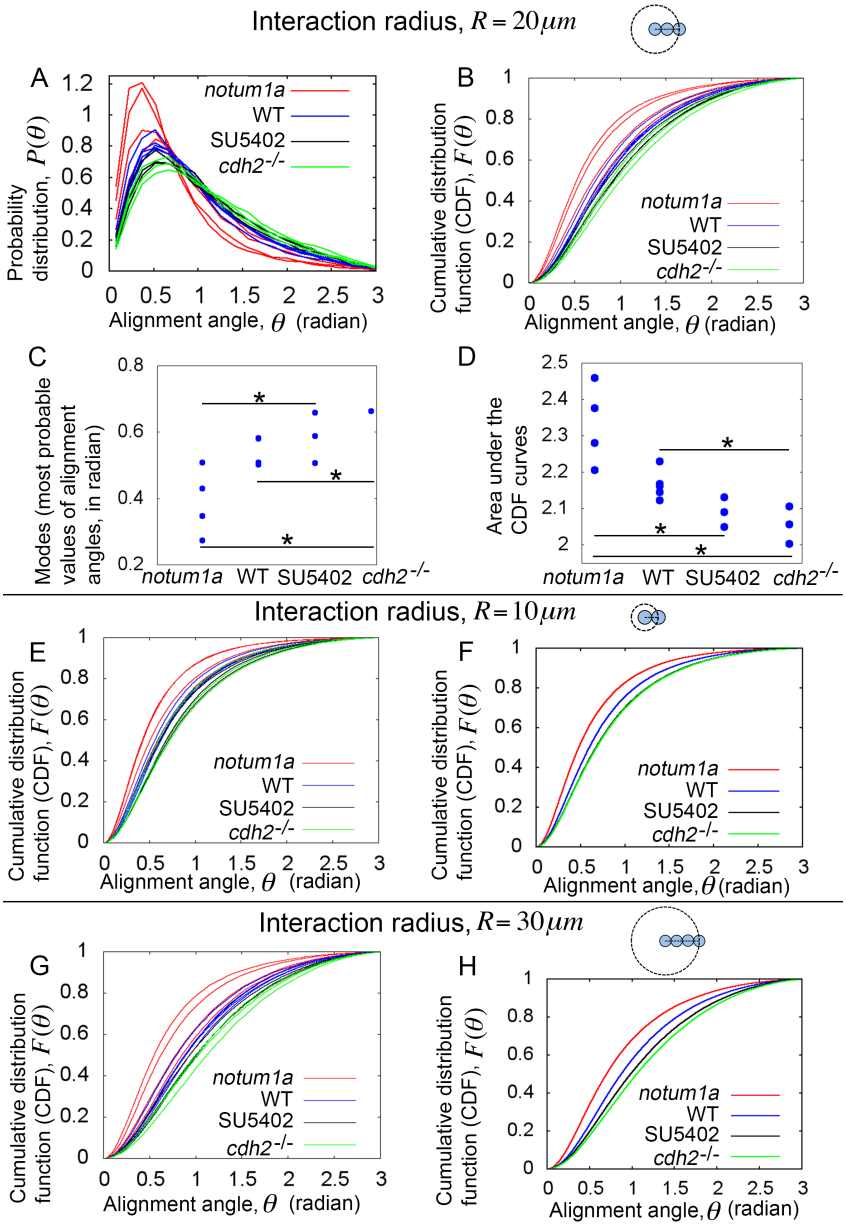

Figure S2. Supplemental statistics of alignment angles of in vivo cell motion; related to Figure 3. (A) Probability distribution functions (PDFs) of alignment angles. Each PDF derives from data from a single embryo. **(B)** Cumulative distribution functions (CDFs) of alignment angles for each individual embryo. **(C)** Modes (most-probable values) obtained from the PDFs of alignment angles, showing lower values for *notum1a* overexpression embryos than other phenotypes. **(D)** Area under the CDF curves for different phenotypes. The p-values are calculated using a two-sample T-test with unequal variance, and "*" denotes $p<0.05$. **(E)** CDFs of alignment angles for individual embryos with interaction radius R=10 microns. **(F)** CDFs of alignment angles for four distinct phenotypes with interaction radius R=10 microns. **(G)** CDFs of alignment angles for individual embryos with interaction radius R=30 microns. **(H)** CDFs of alignment angles for four distinct phenotypes with interaction radius R=30 microns.

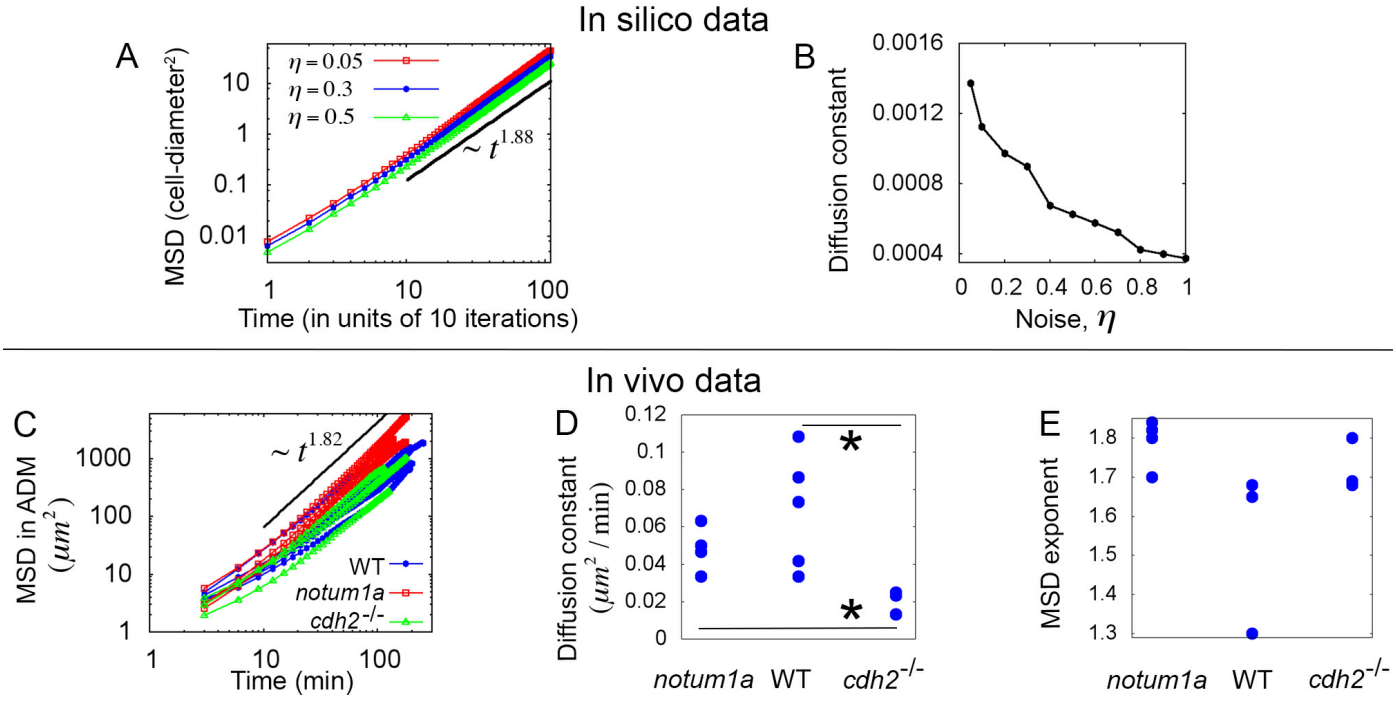

Figure S3. Supplemental analysis of mean-square-displacement (MSD) in the ADM; related to Figure 4. (A) MSD versus lag time from the simulation data is shown in log-log plot for different values of the noise parameter. The black straight line indicates a power-law fitting of the form $4Dt^{\alpha}$, where D is the diffusion constant and α is the MSD exponent. The value of the exponent (1.88) indicates super-diffusive motion. **(B)** The diffusion constant (extracted from the power-law fitting as shown in A) versus noise from in silico simulations. **(C)** For each wild-type, *notum1a* and *cdh2*$^{-/-}$ embryo, the MSD inside the ADM versus lag time is shown in log-log plot. The value of the exponent (1.82) indicates super-diffusive motion similar to our simulations. **(D)** In vivo diffusion constants (as extracted from the power-law fitting of the curves in (C) for different phenotypes. The p-values are calculated using a two-sample T-test, and "*" denotes $p<0.05$. **(E)** In vivo MSD exponents for different phenotypes.